# Electron transport and magnetic studies of $Cu_{100-x}Mn_x$ binary alloys

A. Banerjee and A. K. Majumdar
*Department of Physics, Indian Institute of Technology, Kanpur 208016, India*
(Received 2 March 1992; revised manuscript received 16 June 1992)

A detailed study of Mn-rich $\gamma$-phase $Cu_{100-x}Mn_x$ with Mn concentration up to 83 at. % has been carried with use of ac-susceptibility, dc-magnetization, and electrical-resistivity measurements. All the concentrated alloys have shown the signature of the spin-glass phase below certain temperatures with antiferromagnetic short-range order. The alloys with more than 73 at. % of Mn have long-range antiferromagnetism at *higher temperatures*. An earlier neutron diffraction study has already proved the existence of long-range antiferromagnetism at *low temperatures* for alloys with Mn above 72 at. %. Thus we conclude that $Cu_{100-x}Mn_x$ is a spin glass with short-range antiferromagnetically coupled clusters up to 73 at. % Mn and beyond that it exists in a mixed spin-glass and long-range antiferromagnetic state below certain temperatures. This may be called a reentrant antiferromagnetism since the *high-temperature phase* is a pure long-range antiferromagnetic phase. We have constructed the magnetic phase diagram for the whole range of composition on the basis of our magnetic study and the earlier neutron diffraction measurements. We have found a $T^2$-$T^{5/2}$-type of magnetic contribution to the electrical resistivity in the spin-glass regime for all the alloys. We propose a scheme to isolate the magnetic contribution to the resistivity for all temperatures and apply it to a nondilute system.

## I. INTRODUCTION

Magnetic systems with mixed positive and negative exchange interactions show highly interesting physical properties and still remain an interesting challenge to physicists. The simplest way to achieve such a system is by a random mixture of 3*d* transition metals in a noble-metal matrix. In the dilute limit, the oscillatory Ruderman-Kittel-Kasuya-Yosida (RKKY) interaction gives rise to both positive and negative exchange interactions. The canonical spin glasses belong to this class of magnetic system. With an increase in the 3*d* transition metal, the interactions become complicated and the system proceeds toward a long-range order. The intermediate state shows either the reentrant or the mixed-phase behavior. $Cu_{100-x}Mn_x$ alloys, in the dilute limit, are canonical spin glasses. They follow the scaling law and, hence, obey the predictions of the single-site mean-field theory. But with an increase in the Mn concentration, a deviation from the scaling law is observed. This clearly indicates the formation of magnetic clusters and the intercluster and intracluster interactions dominate the physical properties of the system. Though $Cu_{100-x}Mn_x$ is a well-studied case in the dilute limit, detailed studies of magnetic and transport properties over the whole range of concentration, especially near the percolation threshold, are far from being complete. The reason for the lack of such investigations is because of the complicated nature of the problem. In spite of the fact that $Cu_{100-x}Mn_x$ forms a solid solution over the whole concentration, the binary phase diagram becomes complicated beyond 25 at. % of Mn and the isophasic ($\gamma$-phase) $Cu_{100-x}Mn_x$ is only in a metastable state. The complex nature of the magnetic structure of $\gamma$-phase Mn, as revealed by neutron diffraction studies, complicates the problem further. On top of these, there is a remarkable dependence of magnetic properties on the metallurgical conditions of the samples. Experimentally, the study becomes more critical near the percolation threshold because, in the absence of a spontaneous magnetization, the separation of the long-range antiferromagnetic phase from the spin-glass phase is not very easy from bulk measurements. These motivated us to study the magnetic and transport properties of these isophasic $Cu_{100-x}Mn_x$ binary alloys having the same metallurgical history with the hope of developing a better understanding of the system over the whole concentration range.

We have studied ac susceptibility ($\chi_{ac}$), dc magnetization ($M$), and electrical resistivity ($\rho$) of $\gamma$-phase $Cu_{100-x}Mn_x$ with 4.4–83 at. % of Mn. On the basis of our measurements, we have constructed a magnetic phase diagram which is quantitatively different from the existing experimental one but compares well with the recently calculated theoretical diagram.

Electrical resistivity measurement is known to be an ideal tool to probe into the zero-field state of magnetic metallic alloys and one which is sensitive to the short-range order. The measured resistivity receives contributions from different physical phenomena and the related ordering. In principle, one can get relevant information about various electron scattering processes if one can isolate the respective contributions from the measured resistivity. But, in practice, it is nearly impossible, at least for concentrated polycrystalline alloys. In the absence of a proper guideline, we suggest a scheme for analysis of resistivity data and effective identification of magnetic scattering for all temperatures. Our study is done on concentrated $Cu_{100-x}Mn_x$ alloys and we believe that it can be extended to other polycrystalline systems as well.

 

## II. THEORY

### A. Magnetic properties

In spite of the plethora of work on spin glasses and reentrant or mixed-phase systems, the agreement between the experimental results and their theoretical interpretations from first-principle theories is far from being satisfactory.[1] The mean-field theories which attempt to visualize the spin-glass transition as an equilibrium phase transition have several drawbacks because of the history dependence and nonequilibrium nature of the low-temperature phase. These theories have identified critical lines in the $H$-$T$ plane which are interpreted as phase transition lines, called de Almeida and Thouless (AT) or Gabay and Toulouse (GT) lines for Ising and Heisenberg spins, respectively. In real systems, identification of these lines with proper constants (exponents) is difficult. Though most of the real systems are Heisenberg-like, they tend to show an Ising-like freezing or AT line. This may be possible with an unidirectional anisotropy in small fields for Heisenberg systems.[2] However, the experimental values of the constants in the AT relation are very different from those of the theoretical predictions. Only very recently the GT-like freezing is observed in dilute $Cu_{94}Mn_6$ at low field and a crossover from transverse to longitudinal freezing is observed at high fields.[3] In general, qualitatively, the shift of the freezing temperature ($T_f$) in external magnetic fields in most of the spin glasses is negative. But we will show that in our system and in some other systems like Pd-Ni-Mn alloys[4] and in amorphous Gd-Al (Ref. 5) systems, the shift of $T_f$ as a function of $H$ can change sign.

With the increase in concentration of magnetic ions we can achieve a mixed or reentrant phase. The existence of a mixed ferromagnetic and spin-glass phase is identified in many metallic systems both theoretically and experimentally. But the identification of a mixed antiferromagnetic and spin-glass phase or a reentrant antiferromagnetic one is rare in both theory and experiment. Our $Cu_{100-x}Mn_x$ alloys have shown mixed spin glass and antiferromagnetism in the high Mn concentration. Looking at the mismatch between the results of the mean-field theory and those of the experiments on the real spin-glass and mixed-phase systems, one is tempted to take resort to some phenomenological theory to explain the experimental results. The most common one is Néel's theory of superparamagnetism,[6] which gives a reasonable qualitative agreement with the experimental results.

In this class of theories the spin-glass transition is not considered to be a true thermodynamic phase transition. It is similar to the phenomenon of blocking of superparamagnetic particles in rock magnetism.[7,8] Here, the magnetic material is considered to be made up of magnetic domains or clusters of various shapes, sizes, and spontaneous magnetization. Each cluster is characterized by an anisotropy energy or a coercive field. Wohlfarth[9] has suggested many possible sources of anisotropy. The anisotropy acts like a potential barrier for the particle or cluster magnetization. The thermal activation of the cluster magnetization over the barrier leads to the relaxation of the remanent magnetization given by

$$M_r = M_s \exp(-t/\tau) , \tag{1}$$

where $M_s$ is the spontaneous magnetization of the cluster and $\tau$ is the relaxation time given by

$$\frac{1}{\tau} = \frac{1}{\tau_0} \exp\left[ -\frac{v H_c M_s}{2 k_B T} \right] . \tag{2}$$

Here $v$ is the volume of the particle, $\tau_0$ is a constant $\simeq 10^{-9}$ s, $H_c$ is the coercive field, $k_B$ is the Boltzman constant, and $T$ is the temperature. Below a certain temperature $T_B$, called the blocking temperature of a given cluster, the relaxation of magnetization becomes difficult. This process of thermal activation and blocking of cluster magnetization can explain many experimental observations. We shall discuss different aspects of these theories while discussing our experimental results. Here we give some results deduced from this class of theories.

Wohlfarth has calculated the magnetic susceptibility which is given by

$$\chi(T) = \frac{C}{T} \int f(T) dT , \tag{3}$$

where $C$ is the Curie constant and $f(T)$ is the distribution of blocking temperatures for the clusters. The physical implication of Eq. (3) is that only those clusters contribute to the susceptibility which are not yet "frozen" or whose blocking temperature $T_B < T$. In the absence of a first-principle calculation of $f(T_B)$, it is estimated[10] from the experimentally measured value of $\chi(T)$ using the relation

$$f(T_B) = \frac{1}{C} \frac{d(\chi T)}{dT} . \tag{4}$$

Murani[11] has reframed Eq. (3) in terms of a distribution of relaxation times of the clusters $N(\tau)$ as

$$\chi(\tau) = \frac{C}{T} \int N(\tau) d\tau .$$

The distribution of relaxation times gives rise to a logarithmic decay in remanent magnetization[12] and hysteresis.[13]

The characteristic time or the probe time $\tau_m$ of a particular measurement decides the blocking temperature $T_B$ of a cluster of volume $v$. The lower the $\tau_m$, the higher is the $T_B$ for a given cluster. This can explain qualitatively the frequency dependence of the peak in the ac-susceptibility curve.[14]

Though the above class of theories can explain many experimental observations, the main criticism comes from the phenomenological origin and the lack of first-principle calculations.

Recently, another phenomenological theory has been proposed for the ordered phase of spin glass.[15] In this theory, the spin-glass phase is made up of magnetic "domains" or "droplets" having a broad distribution of excitation energies. The dynamics in spin glasses is dominated by the thermally activated growth or decay of these ordered domains.

### B. Electrical resistivity

We will now mention some calculations done on the transport properties of spin glasses. Rivier and Adkins[16] have obtained a $T^{3/2}$ type of magnetic contribution to the resistivity in spin glasses at low temperatures. Their results are deduced from the calculation of scattering of conduction electrons by the elementary excitation in spin glasses which are the spin-diffusion modes. This $T^{3/2}$ temperature dependence of resistivity has been used to explain the experimental resistivity behavior of canonical spin glasses.

Fischer[17] calculated the resistivity of spin glasses from the scattering of conduction electrons by the static disorder of the impurity spin and by the low-temperature spin excitations. The exchange interaction between the conduction electrons and the spins of the magnetic impurity leads to elastic and inelastic scattering. The elastic contribution is determined from the atomic positions as well as the frozen-in spin configuration. The inelastic contribution is determined by the dynamics of the impurity spins. Taking into account the spin-diffusive modes, the resistivity is calculated to be of the form[17]

$$\rho(T)=\frac{m^*}{ne^2}c\pi N(0)\left\{V^2+\frac{J^2}{4}\left[q(T)+\frac{18}{\pi}\chi\left[\frac{(k_BT)^2}{k_0^2D}J_2-\frac{\pi(k_BT)^{5/2}}{2\sqrt{2}(k_0^2D)^{3/2}}J_{5/2}\right]\right]\right\}, \tag{5}$$

where $m^*$ is the effective mass of electrons, $n$ is the conduction electron density, $N(0)$ is the density of states near the Fermi level, $c$ is the concentration of magnetic ions, $V$ is the spin-dependent potential, $J$ is the exchange interaction, $q(T)$ is the spin-glass order parameter, $k_0$ is the wave vector for electrons in the conduction band, $D$ is the diffusion constant, and

$$J_n=\int_0^\infty dx\frac{x^n}{(e^x-1)(1-e^{-x})}\ .$$

In Eq. (5), $\chi$ is taken to be the temperature-independent equilibrium susceptibility of the spin glass. Hence, in Fischer's theory, the temperature dependence of electrical resistivity of spin glasses, below the transition temperature ($T<T_f$), is of the form $AT^2$-$BT^{5/2}$ with the constants $A,B>0$. This form is valid for spin glasses where there is no ferromagnetic clustering or ferromagnetic short-range order.

## III. EXPERIMENT

The $Cu_{100-x}Mn_x$ alloys with $x=4.4$, 9, 36, 46, 55, 60, 73, 76, and 83 were prepared by induction melting in a pure argon atmosphere of spectroscopically pure Cu and Mn obtained from Johnson-Mathey, Inc. (England). The ingots were homogenized at a high temperature (based on the binary phase diagram and the particular composition), again in a pure argon atmosphere for two days. Then they were swaged, cold rolled, and cut into required shapes. The sample pieces were then sealed in a quartz capsule in an argon atmosphere and heated for a day in a vertical furnace at a temperature close to their respective melting points and then quenched fast in brine. This heat treatment is very important since it helps to remove the defects introduced during the cold work, preserves the high-temperature crystallographic phase ($\gamma$ phase) and introduces random substitutional disorder preventing any possible chemical clustering. After these steps the chemical compositions were checked by chemical and spectroscopic analyses. The powder x-ray-diffraction patterns were recorded using a Rich Seifert IsoDebyeflex 2002 diffractometer. The scanning electron microscope was used to look for any unwanted second phase in the samples.

The ac susceptibility $\chi_{ac}$ was measured by a homemade ac-susceptibility bridge[18] in a 2-Oe rms ac field of frequency 313 Hz from 20 K to room temperature, and in external dc fields between 0 and 280 Oe.

The dc-magnetization measurements were carried out with a Princeton Applied Research Inc. (USA), model 155 vibrating sample magnetometer (VSM). The magnetic field with a maximum of 18 kOe was provided by a 15-inch Varian V-3800 electromagnet. We have used a Janis model 153 variable temperature cryostat with liquid nitrogen to measure magnetic moments from 77 to 300 K. The high-temperature measurements from 300 to 900 K were carried out using a model 151 high-temperature oven assembly in place of the cryostat. The VSM was calibrated against a standard Ni sample and paramagnetic $Er_2O_3$ before any measurement. The cryostat is equipped with a copper-constantan thermocouple but we have also attached a platinum resistance thermometer to the sample rod rather close to the sample for more accurate measurements of temperature. We can maintain the temperature of the sample zone at a constant value within 0.2 K.

Besides these, some magnetic measurements were done in KFK, Karlsruhe using a Faraday balance (Oxford Instruments) and in IIT, Madras using a SQUID magnetometer (Quantum Design). Both are equipped with superconducting magnets. These measurements were done using liquid helium.

We have measured the magnetization ($M$) as a function of temperature ($T$) for $x=36$–$83$ at.% alloys in magnetic fields ranging from 500 Oe to 15 kOe. For all the samples the temperature range was liquid nitrogen temperature almost up to room temperature and for $x=83$ we have gone up to 700 K to find the Néel temperature.

To obtain $M$ versus $T$ curves, we have taken two different routes. First, we cooled the sample in the absence of any magnetic field to the lowest temperature.

Then the field was switched on and the measurement $M(T)$ started as the sample was warmed up. This path is called the zero-field-cooled (ZFC) branch of $M(T)$. The second path is known as the field-cooled (FC) branch of $M(T)$. Here, we cool the sample from room temperature in the presence of a magnetic field to the lowest temperature. Then keeping the field constant we warmed up the sample and measured $M(T)$ in the same field. We call $M/H$ the dc susceptibility $\chi_{dc}$, where $H$ is the measuring field.

To measure the time dependence of magnetization, we have cooled the samples in the presence of a 15-kOe field from room temperature to a temperature $T$ which is much below the temperature where the peak of $\chi_{dc}$ occurred. Then we switched off the magnetic field and started measuring magnetization with time ($t$) in the residual field of the electromagnet ($\sim$30 Oe), keeping the temperature constant. The temperature $T$ was almost the same for all the samples. We have taken the data for $t > 10$ s, since the integration time constant of the instrument is 1 s. Although it was very difficult to measure the time-dependent magnetization for the sample with $x = 76$ because of the small signal, nevertheless a qualitative decay of $M$ with time could definitely be observed at 77 K. However, subsequent measurements with the SQUID magnetometer established the decay of magnetization with time for samples with $x = 76$ and 83 at 4 K.

$M$ versus $H$ for all the samples at room temperature and at the lowest temperature were also measured. $M$ versus $H$ for the sample with $x = 73$ in the ZFC state at 5, 120, and 300 K were carried out in fields up to 55 kOe in the SQUID magnetometer.

Apart from these, $M(T)$ measurements were also carried in samples with $x = 73$ and 76 in a Faraday balance. These measurements were made in the zero-field-cooled state. $M(T)$ was measured in a 1-kOe field from 30 K to room temperature. The $M$ versus $T$ measurements for $x = 76$ and 83 were also carried out in the FC and ZFC states at a 10-kOe field from 5 to 300 K in the SQUID magnetometer.

The electrical resistivity was measured in an automated four-probe dc-resistivity setup from 8 to 300 K.[19] The relative accuracy of the resistance measurement is better than one part in $10^5$ and the temperature stability is $\pm 0.1$ K.

## IV. RESULTS AND DISCUSSION

### A. Ac susceptibility

#### 1. Temperature dependence

Figure 1 shows spin-glass cusps for samples with $x = 4.4$ and 9. The inset shows $\chi_{ac}$ versus $T$ in zero and external dc magnetic fields for the sample with $x = 36$. Figure 2 similarly shows $\chi_{ac}$ versus $T$ for the sample with $x = 46$ in an external dc field of 0 and 280 Oe. We may note here that for all the samples with $x \geq 36$, $\chi_{ac}$ versus temperature curves show a broad peak at high temperatures ($\sim$150 K) except for $x = 83$. The peak value of $\chi_{ac}$ decreases monotonically with the increase in Mn concentration for $x > 9$. In Table I we have listed the variations of the peak values of $\chi_{ac}$ and the peak temperature $T_f$ with concentration.

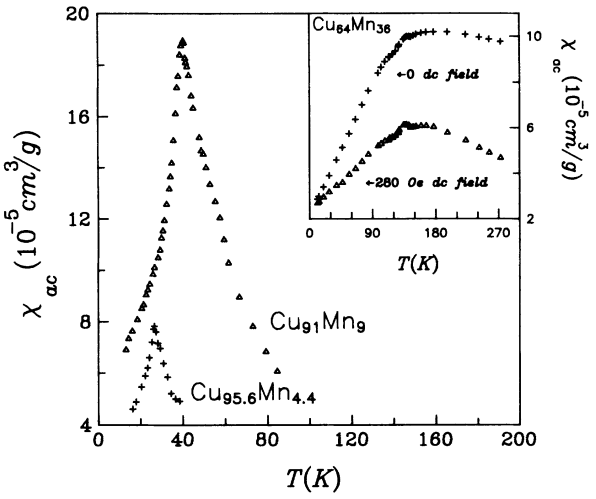


FIG. 1. Temperature dependence of ac susceptibility ($\chi_{ac}$) for $x = 4.4$ and 9 in a zero dc field. The inset shows the temperature dependence of $\chi_{ac}$ for $x = 36$ in zero and 280 Oe fields.

The origin of the peaks being ascribed to antiferromagnetic long-range order or other long-range orders is ruled out on the basis of the high-field dc measurements which will be discussed later. Guy[12] has shown that there is no great significance attached to the sharpness of the peaks even in canonical spin glasses like AuFe (Fe from 0.25 to 7 at. %). His experiments with AuFe in low dc fields make this point clear. The sharpness seems to be a question of temperature scale and here we have gone only up to $\sim 2T_f$. For our samples any temperature above 300 K is almost forbidden because the samples are crystallo-

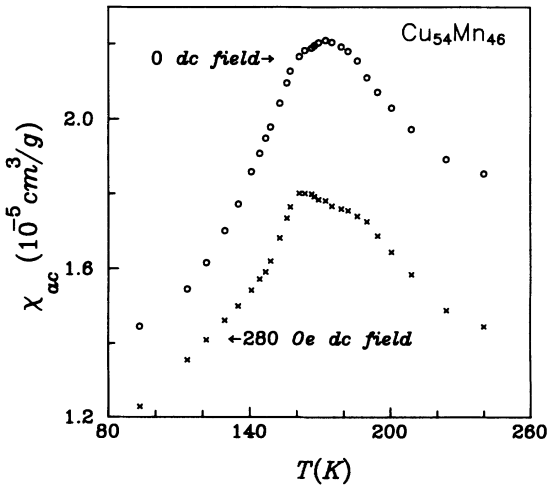


FIG. 2. Temperature dependence of ac susceptibility ($\chi_{ac}$) for $x = 46$ in zero and 280-Oe dc fields.

TABLE I. Mn concentration ($x$) dependence of maximum value of ac susceptibility ($\chi_{ac}^{max}$) and freezing temperature ($T_f$).

| Mn concentration $x$ (at. %) | $\chi_{ac}^{max}$ ($10^{-5}$ cm$^3$/g) | $T_f$ (K) |
|---|---|---|
| 4.4 | 7.7 | 26 |
| 9 | 19.0 | 39 |
| 36 | 10.5 | 160 |
| 46 | 2.2 | 175 |
| 55 | 0.92 | 165 |
| 60 | 0.74 | 165 |
| 73 | 0.76 | ~170 |
| 76 | 0.6 | ~150 |
| 83 | 0.4 | |

graphically metastable and a second phase crystallizes above room temperature.

It is difficult to explain some of the observations such as the broad peak in $\chi_{ac}$ versus temperature, a non-Curie-Weiss behavior above the peak temperature, etc., on the basis of a phase transition or a cooperative phenomenon involving a single order parameter. Here we attempt to understand the results of $\chi_{ac}$ measurements in the framework of the superparamagnetic cluster model described in Sec. II. A typical distribution of blocking temperatures $f(T_B)$ is shown in Fig. 3. This we have calculated from Wohlfarth's model[8,10] for our $x=55$ sample using Eq. (4).

The peak in $\chi_{ac}$ versus $T$ indicates the presence of competing processes and it is a matter of one winning over the other. In this case it is the anisotropy energy of individual clusters versus the thermal energy. According to Néel's model, each cluster has an intrinsic or spontaneous magnetization $M_s$. The magnetic moment $vM_s$ (where $v$ is the volume of the cluster), in the absence of any applied magnetic field, can take up two orientations of equal energy: $\theta=0$ and $\theta=\pi$ with respect to the anisotropy axis of the cluster. The height of the potential barrier between these two states is given by $vH_cM_s/2$ (where $H_c$ = coercive field for the given cluster). Now, if the height is very large compared to the thermal energy $k_BT$, thermal fluctuations cannot move the magnetic moment from one position to the other. So, it always remains fixed in the direction in which it was originally brought by a magnetic field. However, since the height of the potential barrier is $vH_cM_s/2$, a value of $v$ can always be found which is so small that its height is of the order of $k_BT$. In that case, thermal fluctuations can cause the moment to change spontaneously from one position to the other. When we come from the high-temperature side of the $\chi_{ac}$ versus $T$ curve, most of these clusters are free because of high thermal energy and their response to the field is randomized by thermal fluctuations. As we decrease the temperature, the response of the superparamagnetic clusters to the field becomes more and more coherent because of the reduction in thermal fluctuations, and the susceptibility increases. With further decrease in temperature, the bigger clusters facing higher potential barriers start getting frozen or blocked because of the nonavailability of the required thermal energy to cross the barriers. As a result they cannot respond to the field and a competition comes into play. On one hand the reduction of thermal fluctuations with the decrease in temperature enhances the susceptibility above $T_f$, and on the other the decrease in thermal energy blocks the bigger clusters where the blocking temperature is higher and so the susceptibility decreases with the decrease in temperature below $T_f$. The result of these two opposing effects is the broad peak in the susceptibility.

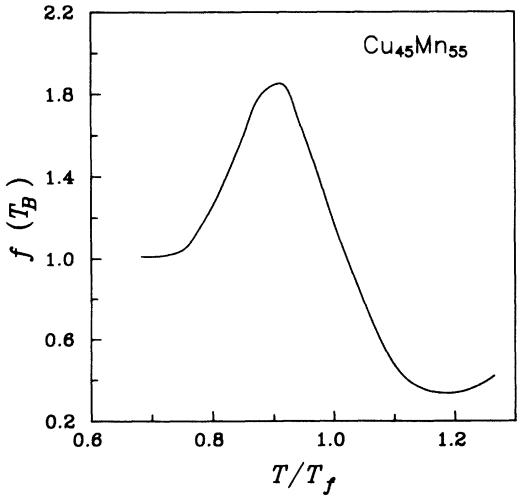


FIG. 3. Distribution of blocking temperature [$f(T_B)$] vs normalized temperature ($T/T_f$) for the sample with $x=55$.

### 2. dc-field dependence

When we look at the results of the effect of dc field on $\chi_{ac}$, we observe that for samples with $x=36$ and 46, $\chi_{ac}$ is always less in the presence of a dc field and this difference persists even at temperatures much higher than the peak temperature. The decrease in $\chi_{ac}$ in the presence of a dc field for all temperatures indicates the existence of short-range order or $d$-$d$ overlap even at temperatures much higher than the freezing temperature. This is more than likely in the concentration range of our present interest. The effect of short-range order, leading to the formation of magnetic clusters, is difficult to handle in first-principle theories of spin glasses. We attempt to understand this effect also on the basis of the phenomenological theory of superparamagnetism.

The external dc field defines the quantization axis of the spins and the ac field excites the spins. To respond to the ac field the spins or the clusters of spins have to reverse their orientation and thus they must lose and gain energy from the lattice, involving spin-lattice relaxation time. Hence, only those clusters can respond to the ac field and contribute to $\chi_{ac}$, whose time constant for spin reversal is less than the time constant of the existing ac field. The relaxation rate $\lambda$ (Refs. 6 and 12) is given by

$$\lambda=1/\tau=1/\tau_0\exp(-E/k_BT)\ ,$$

where $E$ is the height of the potential barrier given by

$$E=(2E_A\pm vM_sH_{\text{ext}})^2/4E_A \ . \tag{6}$$

Hence, we see that the application of a dc field parallel to the ac field increases the time constant for spin reversal and thus causes the decrease in $\chi_{\text{ac}}$ (Figs. 1 and 2). When $\tau$ becomes longer than a typical measuring time $\tau_m$, then the moment is frozen. The blocking temperature ($T_B$) can be found out from

$$E(T_B)=k_BT_Bln(\tau_m/\tau_0) \ . \tag{7}$$

Our results on the effect of the dc field on $\chi_{\text{ac}}$ shows that the blocking temperature has wide distribution over the whole temperature range and confirms the result of our calculation of $f(T_B)$ from the data of $\chi_{\text{ac}}$ in one of our samples (Fig. 3). This broad distribution of $T_B$ justifies the broad peak in $\chi_{\text{ac}}$ and the effect of the dc field on $\chi_{\text{ac}}$. The peak in $\chi_{\text{ac}}$ versus $T$ is described on the basis that $T_f$ is the temperature at which roughly maximum number of spins get blocked. Figure 4 shows that the dc-field dependence of $\chi_{\text{ac}}$ is more pronounced at higher temperatures. The barrier height $E$, at a given temperature, increases as $vH_{\text{ext}}$ where $v$ is the volume of the cluster [Eq. (6)]. At lower temperatures, only smaller clusters respond to the ac field, contributing to the susceptibility and thus the change in $E$ is not significant for these clusters. At higher temperatures, on the other hand, larger clusters are also involved and the change in $E$ shows up through a decrease in $\chi_{\text{ac}}$ with the dc field.

When we look at the peak values of $\chi_{\text{ac}}$, we observe a decrease in the peak susceptibility with increase in the Mn concentration. Though we have added more magnetic atoms, the decrease in susceptibility value at the peak indicates that the addition of more magnetic atoms only serves to cancel the magnetic moments of one another; that is, they are orienting themselves antiferromagnetically. Hence, we conclude that within the magnetic clusters, the spins are antiferromagnetically ordered.

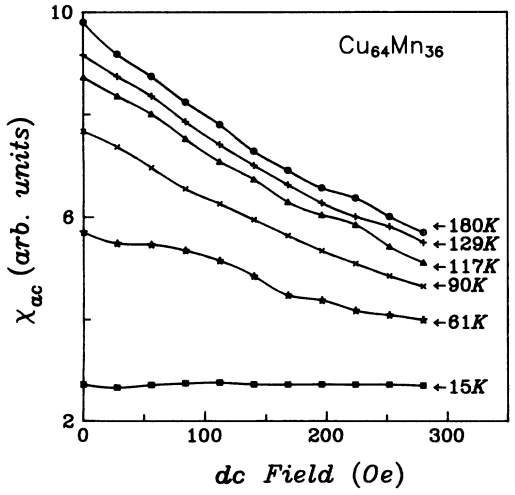


FIG. 4. The external dc-field dependence of $\chi_{\text{ac}}$ for $x=36$ at different temperatures.

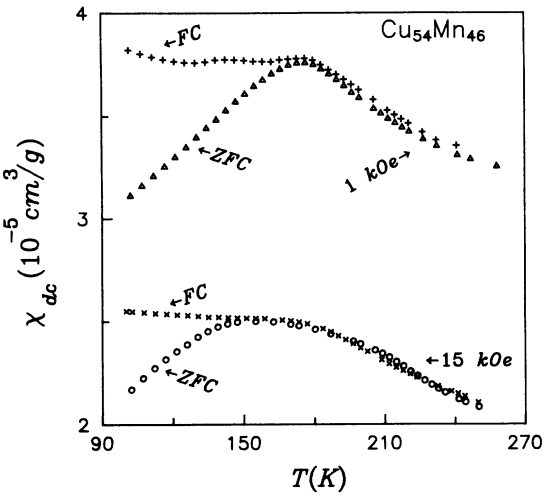


FIG. 5. Temperature dependence of dc susceptibility ($\chi_{\text{dc}}$) for the sample with $x=46$. FC and ZFC stand for field-cooled and zero-field-cooled states, respectively.

### B. Dc magnetization

#### 1. Temperature dependence

In Fig. 5 we have plotted representative $\chi_{\text{dc}}$ versus $T$ curves for the sample with $x=46$ in a 1- and a 15-kOe field. Figure 6 and its inset show the $\chi_{\text{dc}}$ versus curves $T$ at 10 kOe for the samples with $x=83$ and 76, respectively. The $\chi_{\text{dc}}$ versus $T$ for the samples with $x=36$–76 show broad peaks for the zero-field-cooled (ZFC) branches, whereas the FC branches tend to flatten out below the peak. The field-cooled (FC) branch can be obtained reversibly but the ZFC branch is not reversible. This history dependence gives an indication of a spin-glass-like freezing. The temperature where the peak in

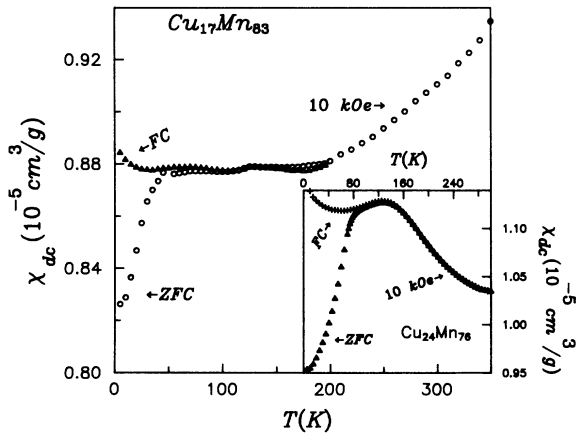


FIG. 6. Temperature dependence of dc susceptibility ($\chi_{\text{dc}}$) for the sample with $x=83$ in a 10-kOe dc field. The inset shows the temperature dependence of $\chi_{\text{dc}}$ for $x=76$ in a 10-kOe dc field. FC and ZFC stand for field-cooled and zero-field-cooled states, respectively.

$\chi_{dc}$ (ZFC) has occurred is determined from $d\chi_{dc}/dT=0$. We call this temperature the freezing temperature ($T_f$). The temperature $T_f$ and the peak value of $\chi_{dc}$, which we call $\chi_{dc}^{max}$, vary with the measuring field and concentration $x$. In the high-temperature side of $T_f(T>T_f)$, both the ZFC and FC branches of the $\chi_{dc}$ versus $T$ curve go together and the plot of $1/\chi_{dc}$ versus $T$ (Fig. 7) shows Curie-Weiss behavior [$\chi=C/(T-\theta)$, where $C$=Curie constant=$N\mu_B^2 p_{eff}^2/3k_B$, $\theta$=Curie-Weiss temperature, $p_{eff}$=effective number of Bohr magneton ($\mu_B$) per Mn atom in units of $\mu_B$, $N$=number of Mn atom/g]. We have determined $p_{eff}$ from the $1/\chi_{dc}$ versus $T$ plot at high temperatures using the Curie-Weiss law. $p_{eff}$ is given by

$$p_{eff}=g[J(J+1)]^{1/2}=\left[\frac{3k_B}{N\mu_B^2\left[\frac{d(1/\chi_{dc})}{dT}\right]}\right]^{1/2}, \quad (8)$$

where $g$=Lande $g$ factor, $J$=total angular momentum of the Mn atom, and $k_B$=Boltzmann constant.

We have fitted our $1/\chi_{dc}$ versus $T$ data to Eq. (8) using a least-squares fitting program, and the lowest temperature of the fitted range is chosen on the basis of the deviation of the data from the Curie-Weiss law by an amount exceeding the experimental error. We have calculated $p_{eff}$ from the slope of the best-fitted straight lines for both the ZFC and FC branches for $H=10$ and 15 kOe, and the *average* value was taken as $p_{eff}$.

Table II gives the variation of $T_f$ and $\chi_{dc}^{max}$, measured at different fields, and $p_{eff}$ with concentration $x$. We have also listed the long-range antiferromagnetic Néel temperature ($T_N$) for $x=76$ and 83. For sample with $x=76$, we observe a small antiferromagnetic peak at 275 K, which is 4% above the background $\chi$ of $\simeq 10^{-5}$ cm$^3$/g (Fig. 8). $x=83$ has an antiferromagnetic Néel temperature at 484 K (inset of Fig. 8).

From Table II we see that $\chi_{dc}$ is very small ($\sim 10^{-5}$cm$^3$/g) and is close to the sensitivity limit of the vibrating sample magnetometer. It becomes rather difficult to predict from our data the existence of a de Almeida and Thouless (AT) line [$(1-T/T_f)\propto H^{2/3}$] or a Gabay and Toulouse (GT) line [$(1-T/T_f)\propto H^2$]. The existence of these lines implies a phase transition in the mean-field theory of spin glasses. It has become more difficult for us to visualize a phase transition, even qualitatively, with an unique Edwards-Anderson (EA) order parameter and its field dependence at $T_f$. The field dependence of the EA order parameter[1] is given by

$$q(T_f,H)\propto 1-\frac{\chi_{dc}^{max}(H)}{\chi_{dc}^{max}(0)}$$

and the related critical exponent $\delta$ is given by

$$q(T_f,H)\propto (H^2)^{1/\delta}.$$

A close look at Table II, where we have listed the variation of $\chi_{dc}^{max}$ with different fields for each sample, will clarify our point. For samples with $x=36$–55, $q$ increases with $H$ corresponding to a positive value of $\delta$, whereas for others $q$ remains more or less constant giving an unphysically large value of $\delta$.

The variation of the peak value of the susceptibility with field is very complicated in nature. Tholence and Tournier[7] have shown that when identical monodomains are cooled from $T>T_B$ to $T<T_B$ the resulting magnetic moment in the direction of the field, in the low-field limit, tends to

$$M=\frac{vM_s^2H}{3k_BT_B} \quad (9)$$

and

$$\chi_{dc}=\frac{M}{H}=\frac{vM_s^2}{3k_BT_B}.$$

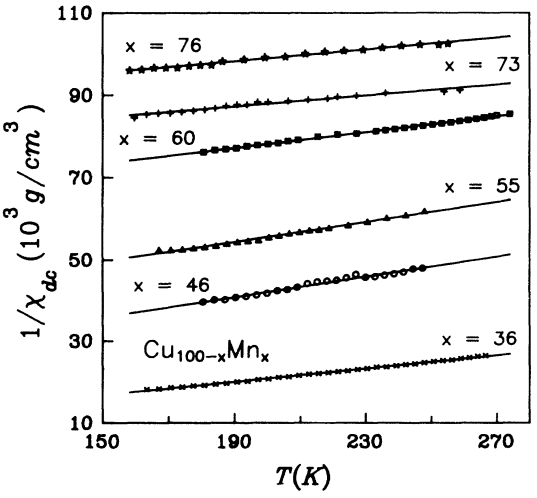


FIG. 7. A typical example of $1/\chi_{dc}$ vs $T$ for each sample in the paramagnetic state.

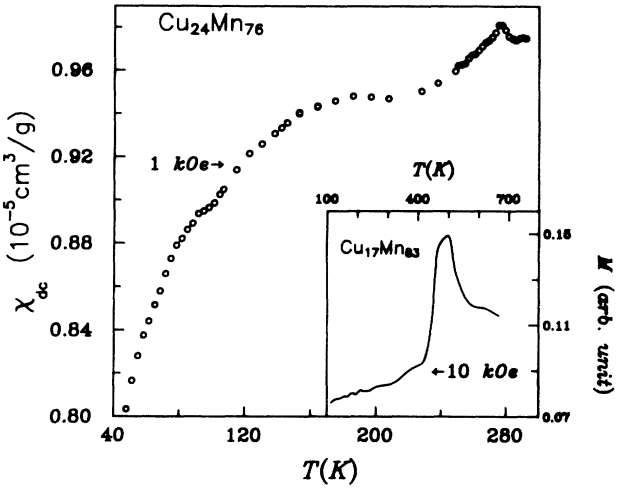


FIG. 8. Temperature dependence of $\chi_{dc}$ for sample with $x=76$ measured in a 1-kOe dc field. The inset shows the temperature dependence of magnetization for the sample with $x=83$ in a 10-keO field.

TABLE II. Mn concentration ($x$) dependence of freezing temperature ($T_f$), maximum dc susceptibility ($\chi_{ds}^{max}$) at different fields, average $p_{eff}$ and Néel temperature ($T_N$).

| Concentration $x$ (at. %) | Field (kOe) | $T_f$ (K) | $\chi_{dc}^{max}$ ($10^{-5}$ cm$^3$/g) | $p_{eff}$ ($\mu_B$) | $T_N$ (K) |
|---|---|---|---|---|---|
| | 1 | 135 | 16.8 | | |
| 36 | 10 | 127 | 5.84 | 0.55 | |
| | 15 | 118 | 6.01 | | |
| | 1 | 176 | 3.77 | | |
| 46 | 10 | 164 | 2.56 | 0.40 | |
| | 15 | 156 | 2.51 | | |
| | 1 | 168 | 2.30 | | |
| 55 | 10 | 164 | 1.83 | 0.31 | |
| | 15 | 156 | 1.91 | | |
| | 10 | 164 | 1.32 | | |
| 60 | 15 | 149 | 1.32 | 0.38 | |
| | 1 | 172 | 1.24 | | |
| 73 | 5 | 164 | 1.16 | 0.43 | |
| | 10 | 159 | 1.15 | | |
| | 15 | 148 | 1.24 | | |
| | 10 | 130 | 1.12 | | |
| 76 | 15 | 145 | 1.15 | 0.42 | 275 |
| 83 | 10 | 45 | 0.88 | | 484 |

Even in this crude approximation the field dependence comes in through $T_B$. The applied field $H_{ext}$ increases the barrier height [Eq. (6)], which in turn increases $T_B$ [Eq. (7)], which results in a decrease of $\chi_{dc}$. Thus, the decrease in $\chi_{dc}^{max}$ with the increase in field for samples with $x=36-55$ can be explained.

From Table II we also see that, for a particular value of the field, $\chi_{dc}^{max}$ has always decreased with the increase in Mn concentration $x$. This can happen either by a decrease in $M_s$ because of more and more antiferromagnetically coupled spins, reducing the uncompensated moment or an increase in $T_B$ because of the increase in anisotropy energy $E_A$ [Eqs. (6) and (7)]. The dominance of the first effect for $x=36-55$ is confirmed by the variation of $p_{eff}$ with $x$, namely, $p_{eff}$ decreases with $x$. But for $x=60-76$, the second effect may be dominant.

Though, with the increase in $x$, we have proceeded toward antiferromagnetism, the complex nature of the antiferromagnetic short-range order in the $x=60-76$ range gives a complicated variation of $p_{eff}$.

The neutron-diffraction study by Cowlam and Shamah[20] in $\gamma$-phase (fcc) $Cu_{100-x}Mn_x$ for $x=72.5-82.5$ shows some interesting features about magnetic short-range order. If $J_1$ is the first-nearest-neighbor interaction and $J_2$ is the second-nearest-neighbor one for Mn, then they have shown that for $x<74$, both $J_1$ and $J_2$ are negative, that is, both are antiferromagnetic. This is called the AF3 structure. Above $x=74$, $J_1$ is negative but $J_2$ is positive, that is, the first is antiferromagnetic while the second is ferromagnetic. This is called the AF1 structure.

From Tables I and II we can see the variations of $\chi_{ac}^{max}$, $\chi_{dc}^{max}$, and $p_{eff}$ with Mn concentration $x$. In this case the decrease in $p_{eff}$ with the increase in Mn concentration up to about $x=55$ shows that the increase in $x$ leads to bigger and bigger antiferromagnetically ordered clusters with lesser and lesser uncompensated spins in the AF3 structure. From $x=55$ to $x=76$, we see an increase in $p_{eff}$ till about $x=73$. This may be due to the change from AF3 to AF1 structure, which is accompanied by a change of $J_2$ from a negative to a positive value. This implies that the increase in $p_{eff}$ is due to the ferromagnetically coupled second nearest neighbor, i.e., the positive $J_2$ in the AF1 structure. Following the above argument the observed $p_{eff}$ should have increased even beyond $x=73$. The constancy of its value for $x>73$ indicates the dependence of both $J_1$ and $J_2$ on Mn concentration $x$ as well as on the small tetragonal distortion observed for $x>74$. Strictly speaking, the decrease in $p_{eff}$ with increasing $x$ should have continued till $x=74$. Our findings seem to suggest that the phase boundary between AF3 and AF1 structures may be quite extended.

Tholence and Tournier[7] have found that the effective moment of a cluster containing $n$ antiferromagnetically coupled spins is given by $\sqrt{n}\,p_{eff}^0$, where $p_{eff}^0$ is the individual magnetic moment of the transition-metal atoms. Hence we can say that $p_{eff}=p_{eff}^0/\sqrt{n}$. From the above relation we can conclude that the observed decrease in $p_{eff}$ with concentration is related to the increase in $n$, the number of spins in a cluster. Therefore, the decrease in $p_{eff}$ for $x=36$ to 55 implies that the average cluster size increases with $x$, i.e., bigger clusters are formed. Since the above calculation does not take care of the change in the sign of $J_2$, which becomes ferromagnetic with the increase in $x$, the small increase in $p_{eff}$ does not mean a decrease in $n$ above $x=60$. Looking at the relative

strengths of $J_1$ and $J_2$ in AF1 structure, we may assume a monotonic increase in the number of spins per cluster or an increase in cluster size.

The shape of the two branches of the $\chi_{dc}$ versus $T$ curve (Figs. 5 and 6) for a spin glass as well as for the alloys of our system can be explained on the basis of Néel's model. When we switch on the magnetic field at $T < T_f$ in the zero-field-cooled branch, only those clusters will respond to the field which have a coercive field less than the applied field or a volume less than some critical volume. The response of all the clusters with $T_B < T$ will contribute to the $\chi_{dc}$. As we increase the temperature, more and more clusters start responding to the field and the resulting $\chi_{dc}$ versus $T$ curve has the same explanation as that of the $\chi_{ac}$ versus $T$ curve. To get the FC branch, we cool the sample in the presence of a magnetic field from high temperature, that is, $T > T_f$. Since at high temperatures most of the clusters are free, they respond to both the magnetic field and the thermal fluctuations resulting in a susceptibility which follows Langevin function $L(vM_sH/k_BT)$ in the ideal case of noninteracting clusters. As we approach the peak from the high-temperature side the clusters slowly proceed toward their blocking temperatures, and under the influence of the external field they get blocked in the direction of the field with the lowering of temperature. So the $\chi_{dc}$ flattens out at low temperatures. Hence we get a different behavior in the FC and the ZFC branches of magnetization where the FC $\chi_{dc}$ is always more than the ZFC $\chi_{dc}$. For the FC curve, the $\chi_{dc}$ below the peak is given by $M_s^2(T)/3K(T)$ for $T < T_B$. Néel has taken the variation of $K$, the anisotropy constant, going as $M_s^2$ for shape anisotropy or magnetocrystalline anisotropy arising from magnetic dipolar interaction within a cluster. In this case the low-temperature $\chi_{dc}$ will be independent of temperature. This is the case with samples with $x = 36$–$55$. But the decrease in $\chi_{dc}$ for $x = 60$–$76$ from the peak value at low temperatures indicates a faster increase in $K(T)$. This may be because of the interaction between the clusters which had been neglected so far. We may note here that this decrease in $\chi_{dc}$ has taken place in the concentration range where $p_{eff}$ has an increase with $x$. So the change in the behavior of $K(T)$ may also have the same origin. The $\chi_{dc}$ versus $T$ curves for the $x = 73$ and 76 samples, taken at 1 kOe, do not show pronounced peaks near $T_f$ as they show in higher fields (Fig. 8). This indicates that there are dipolar interactions within the clusters which get suppressed as we apply higher fields. A similar result was obtained in AuFe spin glasses near the percolation threshold.[21]

### 2. *Time dependence*

A time-dependent magnetization is not an unique property of canonical spin glasses only. It is observed for ferromagnetic and superparamagnetic clusters as well,[22] where the change in magnetization with time is given by

$$M = M_0 e^{-\lambda t} ,$$

where $\lambda$ is the relaxation rate. This type of change in magnetization involves a single relaxation time or barrier height with a constant energy. However, in real systems this type of decay is not observed. To overcome this problem Street and Wooley[23] considered the change in magnetization with time involving a distribution of relaxation times or a distribution of energy barriers $[f(E,t)]$. When we apply their treatment to our case we find, assuming that $f_0(E)$ is independent of $E$, that

$$M = M_0 - S \ln t , \tag{10}$$

where $S \propto \langle m \rangle$ and $\langle m \rangle$ is the average magnetization. Gaunt[24] has shown that the variation of magnetization with time can be approximated by a $\ln t$ variation even when $f_0(E)$ is not constant for time up to 1000 s. Figure 9 shows that, for our samples, Eq. (10) or the $\ln t$ variation is obeyed even for time much longer than 1000 s. Hence the approximation, that the number of barriers is the same for all energies, is not a bad one for our alloys.

We have fitted our data to Eq. (10) for time above 40 s by a least-squares fitting program and found a good fit with normalized mean-squared deviation $\chi^2$ values consistent with the experimental accuracy. The fitted values of $M_0$ and $S$ for different samples are given in Table III. One should note here that since $M$ in Fig. 9 is multiplied by constants for some samples, the apparent slopes in the figure will not match with the values of $S$ in those cases. From Table III we see a monotonic decrease in the value of $S$ with Mn concentration. This signifies that the rate of change of magnetization decreases with the increase in Mn concentration. Néel has taken the height of potential barrier $E = vH_cM_s/2$. With the assumption of a single relaxation time, we can show that the rate of change of magnetization is proportional to $\exp(-vH_cM_s/2K_BT)$. Hence, the increase in Mn concentration leads to an increase in the volume of the clusters. This justifies our earlier conclusion that an increase in $x$ increases the average number of spins in the clusters. One may even try to justify this from the monotonic decrease of $M_0$ with the increase in $x$.

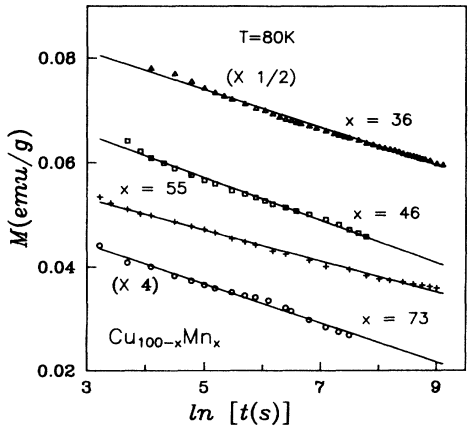


FIG. 9. Remanent magnetization ($M$) at 80 K vs logarithm of time ($t$) where $t$ is measured in seconds. The best-fitted straight lines are shown. $M$ of $x = 36$ and 73 are multiplied by factors $\frac{1}{2}$ and 4, respectively. Thus the slopes are not real ones.

TABLE III. Mn concentration ($x$) dependence of fitted $M_0$ and $S$ of Eq. (10).

| Mn conc. $x$ (at. %) | $M_0$ (emu/g) | $S$ (emu/g) |
|---|---|---|
| 36 | $1.82\times10^{-1}$ | $6.9\times10^{-3}$ |
| 46 | $7.55\times10^{-2}$ | $3.8\times10^{-3}$ |
| 55 | $5.96\times10^{-2}$ | $2.7\times10^{-3}$ |
| 73 | $1.44\times10^{-2}$ | $1.0\times10^{-3}$ |

### 3. *Field dependence*

The zero-field-cooled $M$ versus $H$ for $x=36$ (Fig. 10) deviates from a straight line and resembles the results of earlier studies on $Cu_{100-x}Mn_x$ with Mn=19 at. %.[25] We observe from Fig. 10 that, for $x=46$–76, the zero-field-cooled $M$ versus $H$ curves are roughly linear and we have not detected any hysteresis. From the inset of Fig. 10 we can see that the linearity holds for $x=73$ at all temperatures even up to a field of 55 kOe. The lack of any structure, especially the absence of saturation, makes any quantitative analysis of the data difficult. We will try to give a qualitative justification of the observed $M$ versus $H$ behavior in the light of the spin-glass domain model proposed by Kouvel and Abdul-Razzaq.[26] They explained the $M$ versus $H$ behavior of reentrant NiMn alloys using this model.

We observe from the inset of Fig. 10 that for $x=73$, $M$ versus $H$ is linear at all temperatures. This suggests that there may not be any qualitative difference in the magnetic ordering of the system with temperature. This is consistent with the isothermal magnetization in the superparamagnetic cluster-blocking model where the dynamics of the clusters are only responsible for magnetic response at all temperatures. The persistence of the linearity for all $H$ and the symmetric (undisplaced) $M$-$H$ loop (not shown) seems to indicate that, at least for the zero-field-cooled state, the bulk magnetization is achieved by rotation of magnetization of domains or clusters and not by displacement of domain walls, and the system is subdivided into randomly oriented domains. This is not unusual since in our system the domains are physically separated.

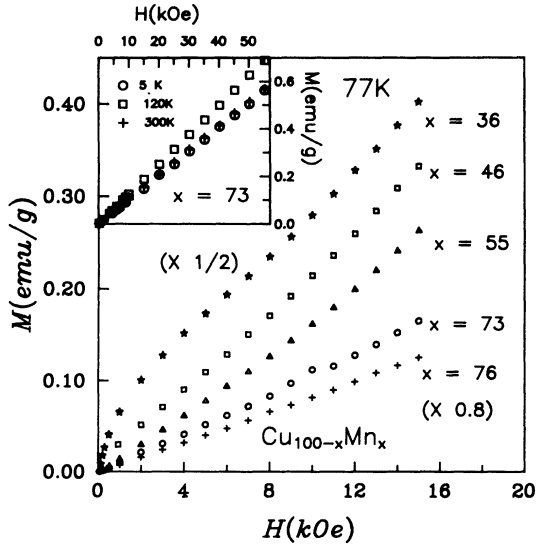


FIG. 10. Magnetization ($M$) vs magnetic field ($H$) of ZFC samples with $x=36$, 46, 55, 73, and 76 at 77 K. $M$ of $x=36$ and 76 are multiplied by factors $\frac{1}{2}$ and $\frac{4}{5}$, respectively. The inset shows magnetization ($M$) versus magnetic field ($H$) of ZFC samples with $x=73$ at 5, 120, and 300 K. Note the overlap of points for 5 and 300 K. ZFC stands for zero-field-cooled state.

To explain qualitatively the linearity of $M(H)$ with the domain model[26] we consider that the domains with average magnetization $M_{av}$ are randomly oriented with average anisotropy field $H_{av}$. The bulk magnetization in a field $H$ can be shown to be given by

$$M(H)=\frac{2M_{av}H}{3H_{av}} \quad \text{for} H\le H_{av} \tag{11}$$

and

$$M(H)=M_{av}\left[1-\frac{H_{av}^2}{3H^2}\right] \quad \text{for } H\ge H_{av}\ . \tag{12}$$

We can see the linearity of $M$ versus $H$ from the limiting case of $H\le H_{av}$ in Eq. (11). It has been shown[26] that the linearity exists even when one assumes a mean-field exchange interaction between the domains.

### C. Magnetic phase diagram

We arrive at the magnetic phase diagram by taking the transition temperatures from our magnetic studies. The spin-glass transition temperatures for $x=4.4$ and 9 are taken from the $\chi_{ac}$ data (Table I) and for others from the $\chi_{dc}$ data at 10 kOe (Table II). The Néel temperatures ($T_N$) for $x=76$ and 83 are also taken from $\chi_{dc}$. This resulting diagram is shown in Fig. 11. We are calling the low-$x$ region spin glass (SG) and the high-$x$ region cluster glass (CG). The transition temperatures and the con-

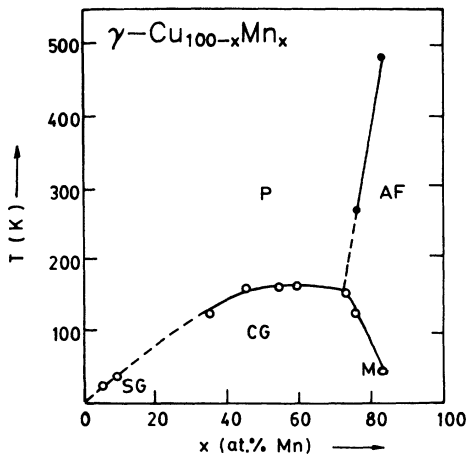


FIG. 11. Experimental magnetic phase diagram for $Cu_{100-x}Mn_x$ alloys. $P$, AF, SG, CG, and $M$ stand for paramagnetic, antiferromagnetic, spin-glass, cluster-glass, and mixed phases, respectively.

structed phase diagram, including the interpolated line from spin glass to cluster glass, have qualitative agreements with those of the earlier studies.[20,27] In the high Mn concentration regime we have found a double transition from the paramagnetic ($P$) to the antiferromagnetic (AF) to the cluster-glass phase for $x=76$. Here, below $T_f$, we have definitely observed some characteristic features of a cluster glass viz. the time and magnetic history dependence of magnetization. If we couple this observation to the neutron-scattering data of Cowlam and Shamah, which show long-range antiferromagnetism even at 4.2 K for alloys in this composition range, then it is clear that below $T_f=130$ K (Table II) the alloys with $x=76$ and 83 exist in a mixed ($M$) antiferromagnetic and cluster-glass phase. Moreover, the alloy with $x=73$ seems to be the multicritical composition with $T_N=T_f=159$ K. However, the actual phase boundary between CG and $M$ seems to be quite fuzzy. One needs to have more alloys in that region. Also, more accurate and sophisticated low-temperature magnetic studies are expected to throw more light on the exact nature of the cluster glass to mixed and antiferromagnetic phase boundaries.

The theoretical magnetic phase diagram has been constructed by Mookerjee and Roy[28] by considering the change in magnetic structure from AF3 to AF1 in the concentration range of 50–74 at. % Mn. We find a good agreement with our experimental phase diagram. However, the sharp decrease in antiferromagnetic to mixed-phase transition temperature observed by us around $x=75$ is not present in the theoretical phase diagram. Moreover, although the authors find double transition above $x=70$, there is no specific mention of the mixed phase in the theory viz. the coexistence of antiferromagnetism and cluster glass. One should mention here that experimentally it is easier to detect the coexistence of ferromagnetism with spin glass from bulk magnetic measurements where one observes both spontaneous magnetization and time and history dependence, as found in $\gamma$-FeNiCr ternary alloys.[29] But in the case of a possible coexistence of antiferromagnetism with spin glass, magnetization measurements alone in polycrystalline samples are unable to prove their simultaneous presence. Neutron-diffraction studies are essential for the detection of the long-range antiferromagnetic order. However, in the case of single crystals it has been possible to prove their simultaneous presence through magnetization measurements only.[30] In the present case of $Cu_{100-x}Mn_x$ alloys, our bulk magnetization measurements supplemented by neutron-diffraction studies establish the presence of mixed antiferromagnetic and cluster-glass phases. We would like to reiterate that, on the basis of neutron diffraction and the present studies, the nature of this phase boundary between cluster-glass and mixed phases is not as clear cut as depicted in some other experimental studies.[20,27] We believe that this phase boundary could lie anywhere within a range of composition as shown in the work of Vedyaev and Cherenkov.[31] However, we have not included this in our phase diagram (Fig. 11) since no work, to our knowledge, throws much light on this boundary.

### D. Electrical resistivity

We present here the results of the electrical resistivity measurements on $Cu_{100-x}Mn_x$ alloys with $x=36$–83 between 8 and 300 K. A typical $\rho(T)$ and $d\rho(T)/dT$ for samples with $x=36$, 73, 76, and 83 are shown in Figs. 12 and 13; the behavior of the rest of the samples is in between. It may be noted here that the experimental error is much less than the width of the data points and the smooth $\rho$ versus $T$ curves are just the raw data and not the smoothed-out data. Such accurate and smooth experimental curves obviously motivate one to do a quantitative analysis of the data and extract as much information as possible. We make an attempt here to analyze the $\rho(T)$ data in spite of the difficulties we face with the metastable state (crystallographic) of our samples and the general problem of interpreting the resistivity data for concentrated polycrystalline alloys. When we tried to measure the resistivity of these alloys above room temperature, we observed a decrease in resistivity from slightly above room temperature. Our x-ray analysis on some of the samples, annealed even at 373 K, shows a change in crystallographic structure with the appearance of an $\alpha$ phase. This has prevented us from measuring the high-temperature resistivity and using the data to extract the lattice contribution independently.

#### 1. Resistivity minima

The alloys with $x=55$–76 show resistivity minima at low temperatures. Earlier studies on the resistivity of concentrated $Cu_{100-x}Mn_x$ alloys have also shown such minima above $x=55$.[32] The existence of resistivity minima in concentrated crystalline alloys and the associated controversies about their origin are quite common but outstanding problems. In an attempt to check whether the minimum has magnetic origin or not, we tried to measure the magnetoresistance in some of these alloys. But the change in resistivity at a 10-kOe field was less than one part in $10^4$ even at the lowest temperature. So

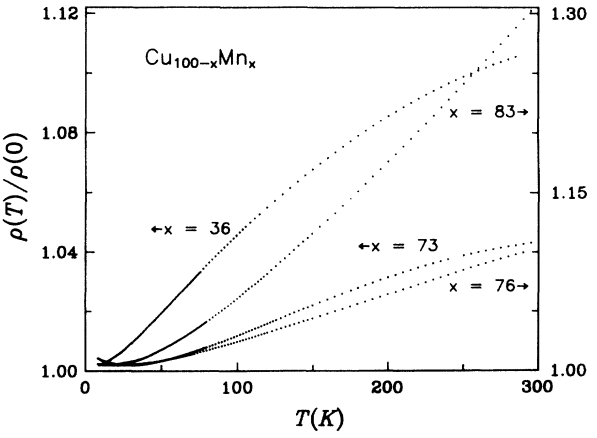


FIG. 12. Temperature dependence of resistivity divided by its minimum value for samples with $x=36$ and 73 (left-hand $y$ axis); 76 and 83 (right-hand $y$ axis).

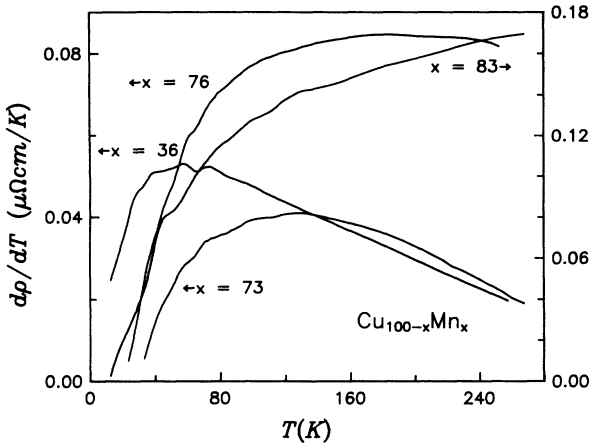


FIG. 13. Temperature dependence of $d\rho/dT$ for samples with $x=36$, 73, and 76 (left-hand $y$ axis) and 83 (right-hand $y$ axis).

we could not arrive at any conclusion on that basis. This negligible change in resistivity in a magnetic field may be because of very low magnetization of the samples.[33] Levin and Mill[34] have considered the effect of spin clusters in the calculation of resistivity for NiCu alloys, and they predicted a resistivity minimum in concentrated crystalline alloys. Rivier[35] has shown the possibility of resistivity minimum in spin glasses. His treatment is based upon the scattering of electrons by spin-diffusion modes and electrostatic potential. The criteria for resistivity minima require strong impurity scattering which is not satisfied by noble-metal–transition-metal canonical spin glasses. Fisher[17] has proposed resistivity minima in spin glasses by combining elastic scattering with inelastic scattering of electrons, but the exact nature of it is not explored. Recently Mookerjee[36] has predicted the existence of resistivity minima in highly resistive alloys ($\rho\simeq 150-600$ $\mu\Omega$ cm) only on the basis of electron-phonon interaction. The high residual resistivity is an indication of electrons being "sluggish" near the Fermi level. These electrons can exchange energy with a phonon bath which will lead to a decrease in resistivity. If $\tau_e$ is the time scale related to the lifetime of electron in the vicinity of an ion and $\tau_0$ is the time scale associated with the ground state of the phonon bath, then as long as $\tau_0 \geq \tau_e$, the electron-phonon coupling will reduce the resistivity. Mookerjee has further shown that with the increase in disorder, the minima in resistivity shift to higher temperatures. Our alloys, having resistivity minima, have $\rho_0$ in the range which satisfies the criterion ($\rho_0\simeq 150-600$ $\mu\Omega$ cm) for a resistivity minimum. The temperature of minima increases monotonically from 10 to 28 K with the increase in $x$ from 46 to 73 accompanied by an increase in $\rho_0$. Since $\rho_0$ can be considered as a measure of disorder, the shift of the resistivity minima to higher temperature with the increase in $\rho_0$ for $x=46-73$ gives us confidence to apply the above theory to our alloys. Though for $x=76$ the value of $\rho_0$ is higher than that of $x=73$, the decrease in the temperature of the resistivity minimum may be because of its higher Debye temperature ($\theta$),[37] which suggests a lower $\tau_0$ and hence the criterion $\tau_0 \geq \tau_e$ is satisfied only at a lower temperature.

### 2. *Resistivity above minima*

Figures 12 and 13 show the following features: (a) $\rho$ versus $T$ curves for $x=36-73$ are $S$ shaped, whereas for $x=76-83$ they are always concave upwards. (b) $d\rho/dT$ versus $T$ curves for $x=36-73$ show broad maxima at $T_{\max}$ which increases with $x$. For $x=76-83$, $d\rho/dT$ increases monotonically with $T$ although very slowly at high temperatures.

Both the above features, namely the $S$-shaped $\rho(T)$ curves and the occurrence of maxima in $d\rho/dT(T)$ are observed in spin glasses.[38,39] These behaviors give indications of possible magnetic contributions to electrical resistivity.

The measured resistivity in these alloys has contributions from different physical phenomena. If we assume the validity of Matthiessen's rule, then the measured resistivity has contributions from static disorder, i.e., the residual resistivity ($\rho_0$), the electron-phonon scattering ($\rho_{\rm ph}$), and the magnetic scattering ($\rho_{\rm mag}$). Hence we can write

$$\rho(T)=\rho_0+\rho_{\rm ph}(T)+\rho_{\rm mag}(T)\ . \tag{13}$$

In the strong-scattering regime near the Anderson localization the Boltzmann formalism breaks down and so is the Matthiessen's rule. This is one of the reasons for concentrating on the higher temperature region, and we apply Eq. (13) above the resistivity minima.

A theoretical calculation for the temperature dependence of resistivity in these polycrystalline materials is very difficult for various reasons. The absence of a proper band-structure calculation poses the main hurdle. So we have tackled the problem in a roundabout way. To estimate the magnetic contribution to resistivity from our measured $\rho(T)$, we have properly taken care of $\rho_0$ and $\rho_{\rm ph}$ and assumed the validity of Matthiessen's rule in the present case. We have taken the standard Bloch-Gruneisen formula for $\rho_{\rm ph}$.[40] The $\rho(T)$ from Eq. (13) becomes

$$\rho(T)=\rho_0+A\left[\frac{T}{\theta}\right]^5\int_0^{\theta/T}\frac{z^5dz}{(e^z-1)(1-e^{-z})}+\rho_{\rm mag}\ , \tag{14}$$

where $\rho_0$ and $A$ are temperature-independent constants and $\theta$ is the Debye temperature.

Rivier and Adkins[16] have shown that for spin glass $\rho_{\rm mag}\propto T^{3/2}$ below the freezing temperature ($T_f$), but Fischer[17] found a magnetic contribution of the form $BT^2$-$CT^{5/2}$ below $T_f$ with constants $B$ and $C>0$. The latter has also remarked that the $T^{3/2}$ variation is due to ferromagnetically ordered spins in the spin glass.

Thus $\rho(T)$ takes the following two different forms due to $\rho_{\rm mag}$ predicted by the above two theories:

$$\rho(T)=\rho_0+A\left[\frac{T}{\theta}\right]^5\int_0^{\theta/T}\frac{z^5dz}{(e^z-1)(1-e^{-z})}+BT^{3/2} \tag{15}$$

and

$$\rho(T)=\rho_0+A\left[\frac{T}{\theta}\right]^5\int_0^{\theta/T}\frac{z^5dz}{(e^z-1)(1-e^{-z})}+BT^2-CT^{5/2}\,. \tag{16}$$

We wrote a program in Pascal which can fit the experimental $\rho(T)$ data to Eq. (14) in general, if we give the value of $\theta$ and the form of $\rho_{\text{mag}}$. We have checked our program by fitting the experimental $\rho(T)$ data for pure gold taken from literature[38] to Eq. (14) with $\rho_{\text{mag}}=0$. Further, we have added different forms of $\rho_{\text{mag}}(T)$ (as for example, $aT^{3/2}$ or $bT^2-cT^3$, etc.) to the $\rho(T)$ value of pure gold and fitted the resulting data to Eq. (14) using our program. We could retrieve the same constants $\rho_0$, $a$, $b$, and $c$, etc., and obtain a normalized mean-squared deviation $\chi^2$ consistent with the accuracy of the data. We have defined the $\chi^2$ of the fit as

$$\chi^2=\frac{1}{N}\sum_{i=1}^{N}\frac{(\rho_{i\ \text{measured}}-\rho_{i\ \text{fitted}})^2}{\rho_{\text{mean}}^2}\,,$$

where $N$ is the number of data points. $\rho_{\text{measured}}$, $\rho_{\text{fitted}}$, and $\rho_{\text{mean}}$ are the measured, fitted, and the mean of the measured values of the resistivity, respectively. The confidence in this kind of fitting is justified by the recent work of Böttger and Hesse[41] in reentrant spin glasses.

We have fitted our experimental $\rho(T)$ data to Eqs. (15) and (16) separately, taking $\rho_0$, $A$, $B$, and $C$ as parameters and $\theta$ of our alloys from literature.[37] The temperature range of the fit is always below $T_f$ (determined from $\chi_{\text{ac}}$ and $\chi_{\text{dc}}$ measurements) and above the temperature of the resistivity minimum. We have tried different temperature ranges within the above specified range. We find that, for alloys with $x=36$, 46, 55, and 83, fitting the data to Eq. (15) gives unphysical signs of the parameters. For the others, the value of $\chi^2$ is less by about a factor of 2 when fitted to Eq. (16). Moreover, as shown in Fig. 14, where deviations of each data point from the best-fitted curves [Eqs. (15) and (16)] for $x=73$ are plotted against $T$, the deviations from Eq. (15) are not only larger but also they show a systematic trend implying a poor fit. In the case of the fit to Eq. (16), the deviation curve cuts the temperature axis much more often. On the basis of this fitting, we conclude that the expression $BT^2$-$CT^{5/2}$ describes the magnetic contribution to the resistivity better in the spin-glass or cluster-glass range ($<T_f$) for our samples. The best temperature range of the above fit is decided on the basis of $\chi^2$ values which are consistent with the experimental accuracy. Table IV summarizes the result of this fitting procedure. Our analysis only establishes the order of magnitude of the constants $A$, $B$, and $C$. Better resolution by an order of magnitude in the measured $\rho(T)$ might throw light on their concentration dependence.

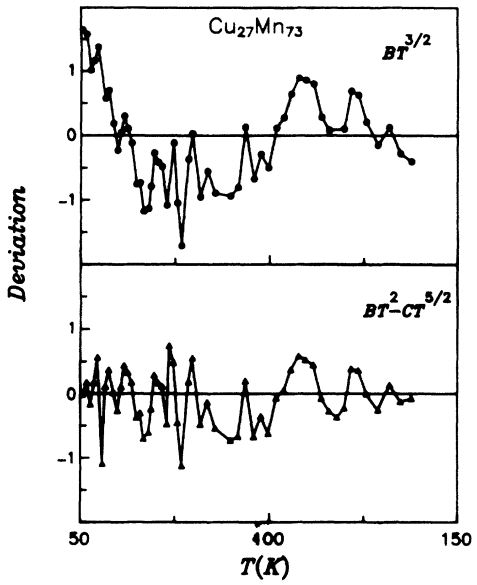


FIG. 14. Deviations of experimental data from the fitted equations with $\rho_{\text{mag}}=BT^{3/2}$ and $BT^2$-$CT^{5/2}$ for the sample with $x=73$.

The justification for our observation of $\rho_{\text{mag}}$ following a $BT^2$-$CT^{5/2}$-type of relation rather than a $BT^{3/2}$-type below $T_f$ can be found in Fischer's original calculations. He has shown that the $T^{3/2}$-type of contribution in resis-

TABLE IV. Mn concentration ($x$) dependence of $\theta$, range of fit, $\chi^2$, and the fitted parameters of Eq. (16).

| Mn $x$ (at. %) | $\theta$ (K) | Range of fit (K) | $\chi^2$ ($10^{-10}$) | $\rho_0$ ($\mu\Omega$ cm) | $A$ ($\mu\Omega$ cm) | $B$ ($10^{-4}$ $\mu\Omega$ cm K$^{-2}$) | $C$ ($10^{-5}$ $\mu\Omega$ cm K$^{-5/2}$) |
|---|---|---|---|---|---|---|---|
| 36 | 325 | 60–90 | 13.8 | 98 | 10.3 | 7.3 | 5.6 |
| 46 | 320 | 80–140 | 25.7 | 139 | 9.0 | 3.0 | 2.0 |
| 55 | 310 | 80–150 | 57.5 | 169 | 5.1 | 1.3 | 0.7 |
| 60 | 305 | 70–150 | 15.9 | 170 | 4.1 | 1.6 | 0.9 |
| 73 | 305 | 50–140 | 7.8 | 196 | 7.1 | 0.8 | 0.2 |
| 76 | 325 | 30–120 | 8.4 | 206 | 11.5 | 3.9 | 1.7 |
| 83 | 360 | 45–110 | 62.3 | 124 | 5.2 | 11.5 | 4.8 |

tivity comes from the ferromagnetic clusters in spin glasses, but our system in no way can be considered to have ferromagnetic clusters. On the contrary, this form of resistivity tends to the Yosida limit[33] of a dilute antiferromagnet ($V^2+S^2J^2/4$) at zero temperature. Along with these, Fischer's calculations hold for systems with a large impurity concentration and in a temperature range where the Kondo effect may be neglected. The range of fit, especially the fitting at higher temperatures, can be rationalized from the physical consideration of spin-diffusive modes which are the source of scattering of conduction electrons. At low temperatures, the spin-diffusive modes may become ineffective for bigger clusters. This is because at low temperatures, the spin waves with wavelength smaller than the cluster diameter will freeze out. The absence of any experimental or theoretical input about the density of states at the Fermi level and the effective mass of electrons forbids us from making any comment about the concentration dependence of the constants $A$, $B$, and $C$ of Table IV. We should note that a good fit for $x=83$ may also indicate the presence of a spin-glass type of spin-diffusive mode in this sample, and hence justify our conclusion regarding the presence of a mixed phase (antiferromagnetic and spin glass) in it (Fig. 12).

The magnetic resistivity above $T_f$ is predicted, using $\rho_0$ and $A$ from the fit below $T_f$ and the $\rho(T)$ data above $T_f$, as

$$\rho_{\text{mag}}(T)=\rho(T)-\rho_0-A\left[\frac{T}{\theta}\right]^5\int_0^{\theta/T}\frac{z^5dz}{(e^z-1)(1-e^{-z})} . \tag{17}$$

$\rho_{\text{mag}}(T)$, thus obtained, shows maxima around 180 K for $x=36$–$60$, moving toward 240 K for $x=73$ and no maximum for $x=76$ and 83 (Fig. 15). The sample with $x=76$, however, shows a decrease in slope around 300 K which may be taken as a precursor to a possible maximum in $\rho_{\text{mag}}$. In contrast, $x=83$ shows that the slope is still increasing around 300 K. In canonical spin glasses the temperature at which $\rho_{\text{mag}}$ is maximum is found to increase with the addition of transition element impurities.[38,39] Inoue and Nakamura[42] have found similar behavior of $\rho_{\text{mag}}$ with maxima around 275 K for $Cu_{100-x}Mn_x$ alloys with $x=16$–$25$. Thus we find that

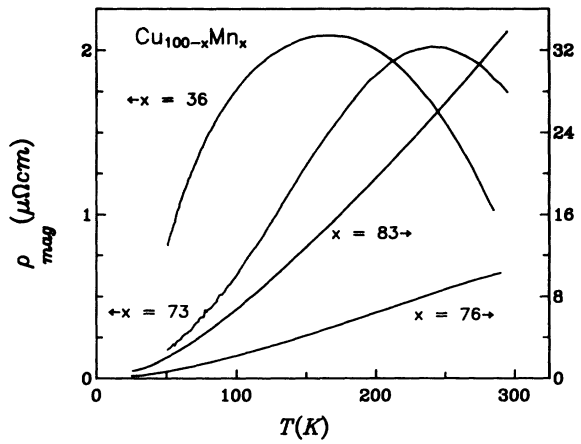


FIG. 15. Temperature dependence of $\rho_{\text{mag}}$ for samples with $x=36$ and 73 (left-hand $y$ axis); 76 and 83 (right-hand $y$ axis).

the occurrence of maximum in $\rho_{\text{mag}}$ in our concentrated alloys is very similar to that of the more dilute ones. One must realize that the extraction of $\rho_{\text{mag}}$ in concentrated alloys is much more difficult, since the estimation of phonon contribution cannot be made directly. However, our solitary attempt in the case of concentrated alloys has met with reasonable success.

The origin of the maximum in $\rho_{\text{mag}}$ has been explained by many authors[38,39,43] in terms of "effective free" and "interacting" moments. For our alloys $\rho_{\text{mag}}$, beyond maximum, falls roughly as $T^2$ as predicted by the theory of Suhl.[44]

For $x=76$, $d\rho/dT$ (Fig. 13) is almost constant for $T>150$ K, implying $\rho_{\text{mag}}\sim T$ or slightly slower since $\rho_{\text{lattice}}\sim T$ at high $T$. For $x=83$, $d\rho/dT$ above 150 K varies more slowly than $T$, implying $\rho_{\text{mag}}\sim T^n$ with $1\le n\le 2$. Any $S$-shaped $\rho(T)$ curve, i.e., $\rho$ varying more slowly than $T$ at high $T$, will yield a maximum in $\rho_{\text{mag}}$ since $\rho_{\text{lattice}}\sim T$ at high $T$. Also, a $\rho(T)$ curve which is linear in $T$ or varies faster than $T$ at high $T$ will have no maximum in $\rho_{\text{mag}}$. In other words, an $S$-shaped $\rho(T)$ curve will have a maximum in $\rho_{\text{mag}}$, whereas a $\rho(T)$ curve which is concave upwards will have no maximum. The composition dependence of the various important quantities is given in Table V.

TABLE V. Mn concentration ($x$) dependence of experimental values, $\rho_{\text{mag}}$ at 300 K, temperatures of the maxima in $\rho_{\text{mag}}$ and $d\rho/dT$.

| Mn conc. $x$ (at. %) | $T_{\min}$ (K) | $\rho_0$ ($\mu\Omega$ cm) | $\rho_{300}$ ($\mu\Omega$ cm) | $\rho_{300}-\rho_0$ ($\mu\Omega$ cm) | $\rho_{\text{mag}}^{300}$ ($\mu\Omega$ cm) | $T(\rho_{\text{mag}}^{\max})$ (K) | $T(d\rho/dT)_{\max}$ (K) |
|---|---|---|---|---|---|---|---|
| 36 | | 97 | 107 | 10 | 1.0 | 180 | 57 |
| 46 | 10 | 139 | 148 | 9 | 0.4 | 180 | 62 |
| 55 | 19 | 169 | 174 | 5 | 0.1 | 175 | 72 |
| 60 | 20 | 170 | 174 | 4 | 0.1 | 190 | 80 |
| 73 | 28 | 196 | 204 | 8 | 1.2 | 240 | 125 |
| 76 | 20 | 206 | 226 | 20 | 11.0 | ~300 | |
| 83 | | 125 | 162 | 37 | 34.0 | >300 | |

The values of $\rho_{mag}$ at 300 K are rather large for $x=76$ and 83 as compared to those for $x=36-73$. This is due to the fact that in contrast to the alloys with $x=36-73$, which have only short-range order, the alloys with $x=76$ and 83 have long-range order (see Fig. 11). A very similar behavior of $\rho_{mag}$ has been observed[38] in AuFe alloys where magnetic resistivity has a sharp increase beyond 17 at. % Fe, which is the percolation threshold from "mictomagnetic" to long-range ferromagnetic phases. It is rather comforting to note that the absolute values of $\rho_{mag}$ at 300 K reported in Ref. 38 agree with those of the present studies in $Cu_{100-x}Mn_x$ (e.g., 43 $\mu\Omega$ cm for 22 at. % Fe in AuFe and 34 $\mu\Omega$ cm for 83 at. % Mn in $Cu_{100-x}Mn_x$ both having long-range magnetic order). From Tables IV and V we see that the best-fitted values of $\rho_0$ and the experimental $\rho_0$ (taken as the minimum $\rho$) are very nearly the same. We further observe that $\rho_0$ increases from 97 to 206 $\mu\Omega$ cm with the increase in Mn concentration from 36 to 76 at. %, which implies an increase in static disorder. At the other end of the concentration ($x=83$) we find a drop of $\rho_0$ to 125 $\mu\Omega$ cm in agreement with Nordheim's rule. The difference between $\rho_{300\ K}$ and $\rho_{0\ K}$ is due to the lattice and magnetic scattering of electrons. This has the same $x$ dependence as that of $\rho_{mag}^{300\ K}$, implying that the lattice contribution does not depend strongly on $x$. This is not unexpected since the Debye Temperature $\theta$ does not depend strongly on $x$ (Table IV).

## V. CONCLUSIONS

The important findings of the present study are briefly summarized below.

(i) Concentration fluctuations *alone* can give rise to the clustering of magnetic atoms in randomly substituted noble-metal–transition-metal binary alloys. The dynamics and the response of these clusters to magnetic fields dominate the magnetic properties of these alloys for all temperatures. This may be evident from the effect of dc fields on $\chi_{ac}$, $M$ versus $H$ behaviors, and, in general, from the variations of $\chi_{ac}$ and $\chi_{dc}$ with temperature.

On an average, bigger and bigger clusters are formed with the increase in Mn concentration $x$. This has been concluded from the concentration dependence of the rate of decay of the time-dependent magnetization. The same conclusion can be reached by coupling the concentration dependence of $p_{eff}$ with the neutron-diffraction results.

The decrease in the peak values of $\chi_{ac}$ and $\chi_{dc}$ with the increase in Mn concentration $x$ and the variation of $p_{eff}$ with $x$ imply the presence of antiferromagnetic short-range order within the clusters. In other words, we conclude that the spins in the magnetic clusters are antiferromagnetically coupled.

(ii) The magnetic phase diagram (Fig. 11) has been obtained on the basis of various magnetic measurements. The alloys with $x \leq 73$ have shown the basic signatures of spin glass viz. time- and history-dependent dc magnetization and peaks in ac susceptibility ($\chi_{ac}$). The low-concentration alloys showing cusps in $\chi_{ac}$ are designated as spin glass (SG), while the concentrated ones showing broad peaks are called cluster glass (CG). For $x=76$ and 83, a double transition from paramagnetic ($P$) to antiferromagnetic (AF) to cluster-glass phases is observed. This, along with the observation of a long-range antiferromagnetic order in neutron-diffraction studies at 4.2 K, leads to the conclusion for the existence of a *mixed* ($M$) phase below $T_f$ ($=130$ K) having properties of both antiferromagnetic and cluster-glass phases. The alloy with $x=73$ seems to be very near the multicritical composition. However, the phase boundaries between CG and $M$ and that between $M$ and Af cannot be clearly defined.

(iii) The resistivity shows qualitatively two different behaviors for $x \leq 73$ and $x > 73$ at high temperatures ($\simeq 300$ K), as are evident from the temperature dependences of resistivity and its temperature derivative (Figs. 12 and 13). This may be taken as an indication that the magnetic ordering is different for these two ranges of composition. The magnetic contribution to the electrical resistivity ($\rho_{mag}$) in the low-temperature range ($<150$ K) for all the samples shows a $BT^2$-$CT^{5/2}$ -type of spin-glass contribution. The estimated $\rho_{mag}(T)$ at high temperature ($>150$ K) shows again two different behaviors for $x \leq 73$ and $x > 73$. The former gives a maximum while the latter increases monotonically with temperature. The large values of $\rho_{mag}$ found for $x=76$ and 83 indicate long-range magnetic ordering in agreement with our phase diagram. Thus we have found in a convincing manner the magnetic contribution to electrical resistivity in a concentrated crystalline alloy system.

In the future one could investigate the nature of various magnetic phase boundaries near the multicritical point by making more alloys with close composition around $x=75$ at. % and studying these low-moment samples using an instrument like the SQUID magnetometer. The so-called mixed phase at the lowest temperatures also deserves detailed investigation.

## ACKNOWLEDGMENTS

We would like to thank Professor A. Mookerjee, Professor K. P. Gupta, and Dr. S. B. Roy for many useful discussions and help at various stages of this work, and Dr. Rita Singhal for help in preparing the revised manuscript. Special thanks go to Professor R. Srinivasan and Professor G. Rangarajan and their group at IIT, Madras, for making their SQUID facilities available to us. Financial assistance of the Department of Science and Technology, Government of India through the Project No. 24(4P-7)/84-STP-II is gratefully acknowledged.

[1]K. Binder and A. P. Young, Rev. Mod. Phys. **58**, 801 (1986); D. Chowdhury, in *Spin Glasses and Other Frustrated Systems* (World Scientific, Singapore, 1987).

[2]G. Kotliar and H. Sompolinsky, Phys. Rev. Lett. **53**, 1751 (1984).

[3]G. G. Kenning, D. Chu, and R. Orbach, Phys. Rev. Lett. **66**, 2923 (1991).

[4]N. G. Hall, R. M. Roshko, and Gwyn Williams, J. Phys. F **14**,

711 (1984).
[5]B. Barbara, A. P. Malozemoff, and S. E. Barnes, J. Appl. Phys. **55**, 1655 (1984).
[6]L. Néel, Adv. Phys. **4**, 191 (1955).
[7]J. L. Tholence and R. Tournier, J. Phys. (Paris) Colloq. **35**, C4-229 (1974); Physica **86-88B**, 873 (1977).
[8]E. P. Wohlfarth, Phys. Lett. A **70**, 489 (1979); J. Phys. F **10**, L241 (1980); S. Shtrikman and E. P. Wohlfarth, Phys. Lett. A **85**, 467 (1981).
[9]E. P. Wohlfarth, in *Magnetism*, edited by G. T. Rado and H. Suhl (Academic, New York, 1963), Vol. 3, p. 351.
[10]C. A. M. Mulder, A. J. van Duyneveldt, and J. A. Mydosh, J. Magn. Magn. Mater. **15-18**, 141 (1980).
[11]A. P. Murani, J. Magn. Magn. Mater. **22**, 271 (1981).
[12]C. N. Guy, J. Phys. F **7**, 1505 (1977); **8**, 1309 (1978).
[13]J. Souletie, J. Phys. (Paris) Colloq. **44**, 1095 (1983).
[14]C. Y. Huang, J. Magn. Magn. Mater. **51**, 1 (1985).
[15]Daniel S. Fisher and David A. Huse, Phys. Rev. B **38**, 373 (1988); **38**, 386 (1988); G. J. M. Koper and H. J. Hilhorst, J. Phys. (France) **49**, 429 (1988).
[16]N. Rivier and K. Adkins, J. Phys. F **5**, 1745 (1975).
[17]K. H. Fischer, Z. Phys. B **34**, 45 (1979).
[18]A. Banerjee, A. K. Rastogi, Manoj Kumar, A. Das, A. Mitra, and A. K. Majumdar, J. Phys. E **22**, 230 (1989).
[19]A. Banerjee, Ph.D. thesis, Indian Institute of Technology, Kanpur, India, 1990 (unpublished).
[20]N. Cowlam and A. M. Shamah, J. Phys. F **11**, 27 (1981).
[21]V. Canella and J. A. Mydosh, Phys. Rev. B **6**, 4220 (1972).
[22]D. J. Dunlop, Rev. Geophys. Space Phys. **11**, 855 (1973).
[23]R. Street and J. C. Woolley, Proc. Phys. Soc. London Sect. A **62**, 562 (1949); Sect. B **69**, 1189 (1956).
[24]P. Gaunt, Philos. Mag. **34**, 774 (1975).
[25]H. Claus and J. S. Kouvel, Solid State Commun. **17**, 1553 (1975).
[26]J. S. Kouvel and W. Abdul-Razzaq, J. Magn. Magn. Mater. **53**, 139 (1985).
[27]P. Gibbs, T. M. Harders, and J. H. Smith, J. Phys. F **15**, 213 (1985).
[28]A. Mookerjee and S. B. Roy, Pramana (to be published).
[29]A. K. Majumdar and P. v. Blanckenhagen, Phys. Rev. B **29**, 4079 (1984).
[30]A. N. Bazhan and S. V. Petrov, in Proceedings of the Indo-Soviet Conference on Low Temperature Physics, Bangalore, India, Jan. 11–14, edited by R. Srinivasan (Indian Institute of Science, Bangalore, 1984), p. 24.
[31]A. V. Vedyaev and V. A. Cherenkov, Zh. Eksp. Teor. Fiz. **91**, 2110 (1986) [Sov. Phys. JETP **64**, 1254 (1986)].
[32]B. R. Coles, Physica **91B**, 167 (1977).
[33]K. Yosida, Phys. Rev. **107**, 396 (1957).
[34]K. Levin and D. L. Mill, Phys. Rev. B **9**, 2354 (1974).
[35]N. Rivier, J. Phys. F **4**, L249 (1974).
[36]A. Mookerjee, J. Phys. Condens. Matter **2**, 897 (1990); **2**, 9399 (1990).
[37]J. L. Zimmerman and H. Sato, J. Phys. Chem. Solids **21**, 71 (1961).
[38]J. A. Mydosh, P. J. Ford, M. P. Kawatra, and T. E. Whall, Phys. Rev. B **10**, 2845 (1974).
[39]I. A. Campbell, P. J. Ford, and A. Hamzić, Phys. Rev. B **26**, 5195 (1982).
[40]J. M. Ziman, in *Electrons and Phonons* (Oxford University Press, London, 1963).
[41]Ch. Böttger and J. Hesse, Z. Phys. B **75**, 485 (1989).
[42]K. Inoue and Y. Nakamura, J. Phys. Soc. Jpn. **29**, 1095 (1970).
[43]A. W. Sheikh and M. El-Fazani, Phys. Status Solidi **147**, 601 (1988).
[44]H. Suhl, Phys. Rev. Lett. **20**, 656 (1968).